mation of multiply charged ions (up to +4) of many elements, such as carbon, nitrogen, oxygen, neon, and argon by strong H I, He I, and He II lines in optically thick nebulae. Moreover, for some ions, the detuning $\Delta\nu$ of frequency ν_1 from the corresponding allowed quantum transition frequency ν_{12} is rather low (<100 cm^{-1}), and the rate of RETPI in the case of such an exact resonance is much higher than for the above considered case of subsequent RETPI in silicon: Si II → Si III → Si IV. We think that the suggested photonic RETPI mechanism is important for understanding the origin of multiply charged ions of many elements inside nebular clouds in the vicinity of bright stars without the requirement of an extremely high ($>50,000$ K) temperature of the central star's photosphere (*1, 2*).

References and Notes

1. L. H. Aller, *Gaseous Nebulae* (Chapman & Hall, London, 1956).
2. B. M. Middlehurst, L. H. Aller, Eds., *Nebulae and Interstellar Matter* (Univ. of Chicago Press, Chicago, 1968).
3. D. E. Osterbrock, *Astrophysics of Gaseous Nebulae and Active Galactic Nuclei* (University Science Books, Sausalito, CA, 1989).
4. I. S. Bowen, *Astrophys. J.* **81**, 1 (1935).
5. M. Göppert-Mayer, *Ann. Phys. (Leipzig)* **9**, 273 (1931).
6. W. Kaiser, C. G. B. Garret, *Phys. Rev. Lett.* **7**, 229 (1961).
7. N. Bloembergen, *Nonlinear Optics* (Addison-Wesley, Redwood City, CA, 1992).
8. Y. R. Shen, *Principles of Nonlinear Optics* (Wiley, New York, 1984).
9. P. A. Franken, A. E. Hill, C. W. Peters, G. Weinrech, *Phys. Rev. Lett.* **7**, 118 (1961).
10. V. S. Letokhov, *Laser Photoionization Spectroscopy* (Academic Press, Orlando, FL, 1987).
11. S. Johansson *et al.*, *Astron. Astrophys.* **361**, 977 (2000).
12. S. Bashkin, J. O. Stoner Jr., *Atomic Energy Levels and Grotrian Diagrams*, vol. 1 (North-Holland, Amsterdam, 1975).

13. One of the authors (V.L.) is grateful to A. Makarov for valuable discussions.

28 September 2000; accepted 13 December 2000

Cherenkov Radiation at Speeds Below the Light Threshold: Phonon-Assisted Phase Matching

T. E. Stevens,[1,2]* J. K. Wahlstrand,[1] J. Kuhl,[2] R. Merlin[1]†

Charged particles traveling through matter at speeds larger than the phase velocity of light in the medium emit Cherenkov radiation. Calculations reveal that a given angle of the radiation conical wavefront is associated with two velocities, one above and one below a certain speed threshold. Emission at subluminal but not superluminal speeds is predicted and verified experimentally for relativistic dipoles generated with an optical method based on subpicosecond pulses moving in a nonlinear medium. The dipolar Cherenkov field, in the range of infrared-active phonons, is identical to that of phonon polaritons produced by impulsive laser excitation.

Cherenkov radiation (CR) is extensively used in experiments for counting and identifying relativistic particles (*1, 2*). The effect derives its name from Pavel Cherenkov (*3*), who, following a suggestion by Vavilov (*4*), discovered in 1934 that substances exposed to fast electrons emit coherent light (*5*). The theory of CR was developed by Frank and Tamm in 1937 (*6*). They showed that charges traveling faster than the speed of light in a substance with a frequency-independent refractive index n emit radiation displaying a shock-wave singularity at the surface of a cone defined by $\cos\theta_C = c/nv$, where θ_C is the angle between the direction of motion and that of the electromagnetic wavefront (the angle subtended by the cone is $\alpha_C = \pi/2 - \theta_C$), c is the speed of light in vacuum, and v is the speed of the particle.

We concern ourselves with CR in an isotropic material whose frequency (Ω)–dependent dielectric constant $\varepsilon = n^2$ in the vicinity of a resonance at frequency Ω_0 can be approximated by the nondissipative Lorentz form

$$\varepsilon(\Omega) = \varepsilon_\infty + \frac{\varepsilon_0 - \varepsilon_\infty}{1 - (\Omega/\Omega_0)^2} \qquad (1)$$

ε_0 is the dielectric constant at $\Omega = 0$, and ε_∞ accounts for the contribution of higher lying excitations. Although analytical expressions for the Cherenkov field of a generic dielectric have been available for a long time (*7*), its properties in the case of a strongly dispersive substance have not been studied in any detail until very recently (*8*). Here, we report on both experimental and theoretical work revealing important qualitative differences for speeds below and above the speed of light at $\Omega = 0$, $c_0 = c/n(0)$ ($v > c_0$ and $v < c_0$ are referred to in the following as the superluminal and subluminal regimes) (*9*). We use subpicosecond optical pulses to generate an optical analog of a relativistic dipole (*10, 11*). Measurements of the Cherenkov electric field **E** for a planar distribution of such dipoles show that the field is nonzero for $v < c_0$ but vanishes for $v > c_0$. We also revisit the standard problem of CR emitted by a point charge and find that, regardless of v, the field pattern is always outlined by a cone. However, the v dependence of θ_C exhibits a minimum $\theta_C = 0$ at $v = c_0$, contradicting the widely held belief that there is a one-to-one correspondence between v and the Cherenkov angle (*1, 2*). Finally, we reinterpret experiments on the ultrafast generation of polaritons (*12–17*) in terms of CR.

A representative set of our calculations is reproduced in Fig. 1. $\varepsilon(\Omega)$ is given by Eq. 1 and the radiation source is moving along the z axis. The magnitude of the field E for a point particle is shown in Fig. 1A (*18*). Because of the symmetry of the problem, the electromagnetic field depends on $z - vt$ (t is the time) and $\rho = (x^2 + y^2)^{1/2}$, but not on the azimuth. The diagrams in Fig. 1B depict E for a collection of electric dipoles uniformly distributed in a plane. Both the dipole moment and the lane are perpendicular to the velocity. The latter case is directly relevant to our experiment.

Consider first the point source. The features of interest are (i) the observation that θ_C is well defined at all speeds (*19*), (ii) the fast oscillations at $v > c_0$ with a frequency that increases with decreasing $\alpha = \tan^{-1}\rho/(vt - z)$, and (iii) the subluminal beats. More importantly, our results indicate that a given Cherenkov angle is connected not with one, but with two particle speeds (one below and one above the light threshold).

For a point charge, the electromagnetic potentials can be expressed in terms of integrals of the form (*7*)

$$A(t - z/v, \rho, v) = \int \Phi(\Omega) e^{-i\Omega(t-z/v)} H_0^{(1)}(s\rho) d\Omega \qquad (2)$$

$H_0^{(1)}$ is a Hankel function, Φ is a slowly varying function of Ω, and $s^2(\Omega) = \Omega^2(\varepsilon v^2/c^2 - 1)/v^2$. At large distances, we can restrict the integration to the radiative range $\Omega_C \le \Omega \le \Omega_0$ where $s^2 \ge 0$; Ω_C is either the frequency at which $v^2 = c^2/\varepsilon$ ($v < c_0$) or $\Omega_C = 0$ ($v > c_0$). Using the asymptotic expression of $H_0^{(1)}$,

[1]The Harrison M. Randall Laboratory of Physics, University of Michigan, Ann Arbor, MI 48109–1120, USA. [2]Max-Planck-Institut für Festkörperforschung, D-70569 Stuttgart, Germany.

*Present address: Veridian ERIM International, Post Office Box 134008, Ann Arbor, MI 48113–4008, USA. †To whom correspondence should be addressed. E-mail: merlin@umich.edu

$$A \approx \int_{\Omega_c}^{\Omega_0} \Xi\,(\Omega) e^{if(\Omega)} d\Omega \approx \sum_{\Omega_i} \sqrt{\frac{2\pi i}{f''(\Omega_i)}}\, \Xi\,(\Omega_i) e^{if(\Omega_i)} \qquad (3)$$

$\Xi = (\pi s\rho/2)^{-1/2}\Phi$, $f = -\Omega(t - z/v) + s\rho - \pi/4$, and f'' denotes the second derivative. The sum is over frequencies $\Omega_i(vt - z, \rho)$ for which $df/d\Omega = 0$, i.e., the solutions to

$$v\,\frac{ds}{d\Omega} = \frac{vt - z}{\rho} = \cot\alpha \qquad (4)$$

that lie within the range of integration.

Equation 4 associates a particular frequency with a conical wavefront moving with the group velocity (*7*). Accordingly, θ_C is defined by the cone that subtends the largest angle or, alternatively, the frequency corresponding to $s'' = 0$. As Eq. 4 has no solutions outside the so-defined cone, the field is expected to vanish (or be negligibly small) outside its boundaries. For $v > c_0$, $\Omega = 0$ is always a solution and, thus, $\theta_C \equiv \cos^{-1}c_0/v$. The corresponding expression for subluminal speeds is

$$\theta_C = \tan^{-1}[4\gamma^{-1}\sqrt{(\eta - \zeta)/\zeta^3}] \qquad (5)$$

where $\gamma = (1 - \varepsilon_\infty v^2/c^2)^{-1/2}$, $\zeta = 2 - (4 - 3\eta)^{1/2}$, and $\eta = 1 - (\Omega_C/\Omega_0)^2$ (*8*, *20*). In agreement with the numerical work, an analysis of the zeros of s'' shows that $d\theta_C/dv > 0$ for $v > c_0$ (same as for nondispersive media), whereas $d\theta_C/dv < 0$ for $v < c_0$. Moreover, the fact that c/n is largest and the phase and group velocities coincide at $\Omega = 0$ accounts for the shock-wave singularity at the cone boundaries in the superluminal case. The reason why the field is nonzero outside (albeit much smaller than inside) the cone in the subluminal regime is that there are frequency components that travel at speeds arbitrarily close to v (*19*). Further reflection shows that Eq. 4 has two roots for $v < c_0$ that come together at the cone boundary, but only one for $v > c_0$. Therefore, the subluminal beats and the superluminal oscillations shown in Fig. 1 simply reflect the fact that Eq. 3 contains two terms for the former but only one for the latter regime. Consistent with the calculations, Eq. 4 also predicts that the superluminal frequency should increase with decreasing α because $s'' > 0$ for $\Omega \neq 0$ and that the beat frequency should also increase as the two roots move farther apart.

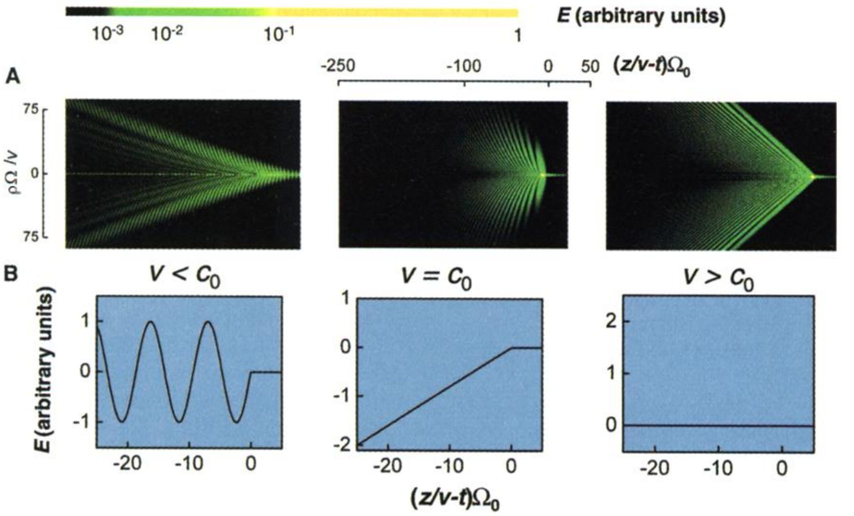

Fig. 1. Calculations for $c_0/c = 0.34$. Left, middle, and right columns correspond to $v/c_0 = 0.88$, $v/c_0 = 1$, and $v/c_0 = 1.47$, respectively. (**A**) Color-scale plot of E for a point particle. (**B**) E versus $(z/v - t)\Omega_0$ for electric dipoles oriented and distributed uniformly in a plane $\perp$ $\mathbf{e}_z$. The field is polarized in the direction of the dipoles.

In our experiments, the radiation source was not a point particle but a spatially extended collection of electric dipoles created by a femtosecond optical pulse (*10*, *11*), referred to hereafter as the pump pulse. This pulse, of central frequency ω_L, moves through the medium with velocity $v = c_g(\omega_L)$ and interacts with itself to generate a low-frequency polarization through frequency-difference generation, a nonlinear effect associated with the susceptibility tensor $\chi^{(2)}$ (*21*); $c_g = d\omega_L/dq$ is the light group velocity and q is the wave vector. The generation of CR by such methods was pioneered by Auston and co-workers (*10*, *11*), who applied the technique to $LiTaO_3$ in a range for which $v \gg c_0$. Close to the pump, and when the pulse lateral spread is much larger than its spatial width, the polarization source can be approximated by an infinitely extended planar object; i.e., the field depends only on $t - z/v$. The Hertz potential for this problem is

$$\mathbf{\Pi}(\Omega) = -\frac{4\pi\zeta e^{-i\Omega(t-z/v)}}{v\varepsilon(\Omega)s^2(\Omega)}\,\mathbf{e}_d \qquad (6)$$

where $\mathbf{e}_d$ is the unit vector in the direction of the dipoles and ζ is the areal polarization. Using $\mathbf{E}(\Omega) = \nabla(\nabla.\mathbf{\Pi}) - (\varepsilon/c^2)d^2\mathbf{\Pi}/dt^2$, and integrating over Ω, we obtain $\mathbf{E} \equiv 0$ for $v > c_0$. For $v \leq c_0$, we also have $\mathbf{E} \equiv 0$ when the dipoles are oriented along z. But, if $\mathbf{e}_d \perp \mathbf{e}_z$, $E \propto \Omega_C^{-1}\sin\,[\Omega_C(t - z/v)]$ and the field is polarized along $\mathbf{e}_d$ (this, for $z < vt$, otherwise $\mathbf{E} \equiv 0$). These results, central to the interpretation of our experiments, are displayed in Fig. 1B. The behavior of E stems from the fact that, at subluminal speeds, $s^2(\Omega_C) = 0$ whereas $s/\Omega \neq 0$ if $v > c_0$.

Our measurements were performed at 10 K on a single crystal of ZnSe. The relevant optical parameters, gained primarily from (*22*), are shown in Fig. 2, A and B (*23*, *24*). ZnSe crystallizes in the noncentrosymmetric ($\chi^{(2)} \neq 0$) zincblende structure showing a triply degenerate optical phonon that is both Raman and infrared active. The coupling be-

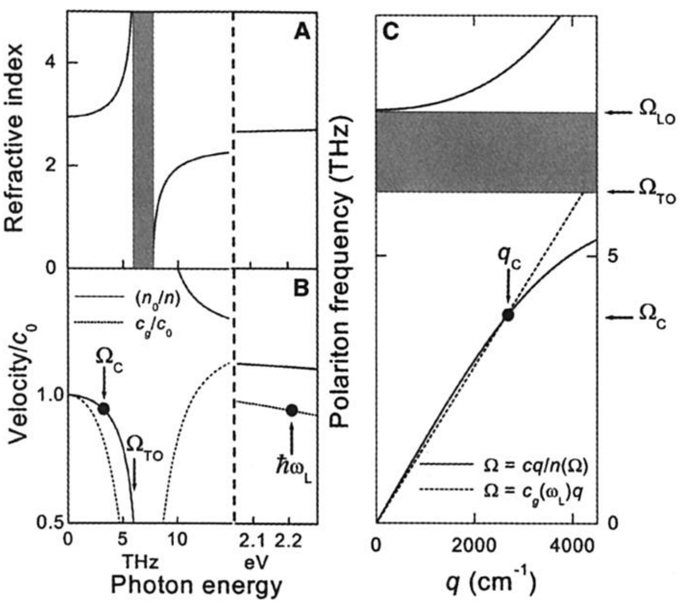

Fig. 2. Optical parameters of ZnSe in the far infrared (units of THz) and visible range (units of eV) at 10 K (*22*). (**A**) Refractive index. (**B**) Phase (solid line) and group (dashed line) velocity relative to $c_0 = c/n(0)$ and (**C**) polariton dispersion. For dipoles created by a pulse of central frequency ω_L, the range of Cherenkov emission is $\Omega_C \leq \Omega \leq \Omega_{TO}$. Shaded areas denote the region between the TO and LO frequencies in which electromagnetic radiation cannot propagate in the absence of damping.

tween infrared-active phonons and the electromagnetic field leads to polaritons (*25*) whose dispersion is shown in Fig. 2C. At large q, the mode splits into transverse (TO) and longitudinal (LO) components of frequencies $\Omega_{TO} \approx 6.3$ THz and $\Omega_{LO} \approx 7.7$ THz. The phonon linewidth at low temperatures is ~0.05 THz $\ll \Omega_{TO}$ (*23*). Hence, far from the anomalous dispersion range, the optical constants of ZnSe are well described by Eq. 1 with $\Omega_0 \equiv \Omega_{TO}$ and $(\Omega_{LO}/\Omega_{TO})^2 = \varepsilon_0/\varepsilon_\infty$. In the visible range (Fig. 2B), n depends strongly on frequency reflecting the band gap at ~2.82 eV (*23*). The dispersion is sufficiently large that $c_g < c_0$ above ~2 eV (*24*). This, together with optical isotropy and lack of inversion symmetry (to ensure that $\chi^{(2)} \neq 0$), makes ZnSe a good choice for subluminal CR experiments.

Our laser system produces 90-fs pulses in the range 1.8 to 2.3 eV by pumping an optical parametric amplifier with a Ti:sapphire regenerative amplifier at a repetition rate of 200 kHz. We used a standard pump-probe setup. The pump generates the Cherenkov field, which we monitor by measuring the transmission of the probe pulse that follows behind (*26*). The difference between the transmission in the presence and the absence of the pump, ΔT, gives a measure of the field strength because it is sensitive to changes in the refractive index due to the same nonlinear interactions that create the field (*24*). The ZnSe sample is a cube with ~5 mm by 5 mm faces perpendicular to the [110], $[1\bar{1}0]$, and [001] directions. Light penetrated the crystal along the [110] z axis to create dipoles with $\mathbf{e}_d \perp \mathbf{e}_z$ (this gives $\mathbf{E} \neq 0$) and, concomitantly, to avoid coupling with the LO phonon. The pump field was oriented at 45° with respect to both the [001] and $[1\bar{1}0]$ axes. This choice gives the largest E and a nonlinear polarization at ~18.4° with respect to the pump field. The average pump and probe powers were 2 and 0.8 mW. The two beams were polarized perpendicular to each other to reduce noise and focused onto a common spot ~100 μm in diameter, a value that is ~10 times larger than the spatial width of the pulses. It is therefore justifiable to apply Eq. 6 to describe the Cherenkov field in the vicinity (although away from the edges) of the pump.

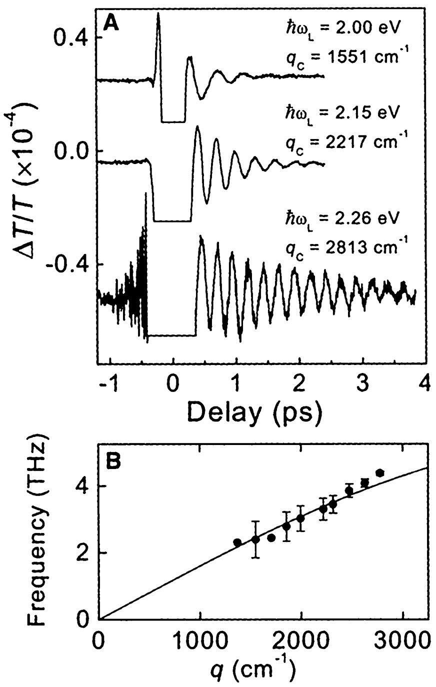

Fig. 3. (**A**) Normalized differential transmission as a function of the pump-probe delay. Values of q were obtained from the data in Fig. 2. A set of points in the vicinity of zero delay were replaced by a baseline to eliminate the so-called coherent artifact peak, which is a few orders of magnitude larger than the oscillation amplitude. The top and bottom traces were shifted vertically by 2.5×10^{-5} and -4.7×10^{-5}. (**B**) Comparison between theory and experiment. The circles give the frequency determined from $\Delta T/T$ and the associated q gained from ω_L through the data of Fig. 2B. The vertical bars represent the inverse of the measured decay time τ. The solid curve was obtained from a fit to the experimental results.

Time-domain results are shown in Fig. 3A. ΔT oscillates at a frequency that increases with increasing ω_L. We emphasize that the oscillations disappear if $c_g > c_0$ ($\hbar\omega_L < 1.97$ eV). From the discussion following Eq. 6, it is clear that such a behavior is consistent with a Cherenkov field created by a quasi-planar distribution of dipoles (Fig. 1B, left). The measured values (Fig. 3B) exhibit very good agreement with the prediction that the oscillation frequency is given by Ω_C, as defined in Fig. 2B. This, and the fact that the selection rules are consistent with the symmetry properties of $\chi^{(2)}$ (*24*), confirm our assignment.

Another feature of interest in Fig. 3 is that the apparent decay time of the oscillations τ increases with ω_L. A straightforward calculation indicates that the trivial dephasing due to the pulse bandwidth is too small to account for τ^{-1} at small frequencies. For various reasons, we believe that this effect is a manifestation of the crossover between one- and three-dimensional behavior, as opposed to the homogeneous broadening of the oscillation. As the probe moves farther away from the pump, we expect that the field will resemble that of a point dipole. This interpretation is supported by the realization that the corresponding decay length of the oscillations, i.e., $c\tau/n(\omega_L)$, is on the order of the diameter of the focal spot. Also note that, contrary to the behavior of the bars in Fig. 3B, polariton lifetimes are generally determined by the lifetime of its phonon component, which becomes less important at lower frequencies where the polariton is essentially an infrared photon.

We now address the issues of phase matching, CR, and polariton generation. Three methods to generate a polarization through $\chi^{(2)}$ processes are shown in Fig. 4. The scheme in Fig. 4A relies on a tightly focused laser beam to produce infrared radiation (*10*, *11*), whereas the (two-beam) traveling-grating method, shown in Fig. 4B, is the approach most commonly used to generate coherent polaritons (*12–17*). What these methods and ours (Fig. 4C) have in common is that the radiation source is a function of $t - z/v$. Given this dependence and the fact that the nonlinear polarization involves terms of the form $\exp[i(\mathbf{k}_2 - \mathbf{k}_1).\mathbf{r}\text{-}i(\omega_2 - \omega_1)t]$ ($\mathbf{k}$ and ω denote the wave vector and the frequency in the Fourier decomposition of the pump pulse), it is a simple exercise to show that a necessary condition for phase matching is $\Delta k_z = \Omega/v$. Using $\mathbf{q} = |\Delta\mathbf{k}|$ and $\Omega = c|\Delta\mathbf{k}|/n(\Omega)$, we find

$$q_\rho/q_z = (n^2v^2/c^2 - 1)^{1/2} \qquad (7)$$

Here, as before, $\mathbf{q}$ and Ω are the polariton wave vector and frequency, $\Delta\mathbf{k} = \mathbf{k}_2 - \mathbf{k}_1$, and q_ρ denotes the component of $\mathbf{q}$ perpendicular to $\mathbf{e}_z$. This condition establishes the link between CR and polariton generation in that, by way of $\tan\theta_C = q_\rho/q_z$, Eq. 7 becomes identical to the expression for the Cherenkov angle. The vari-

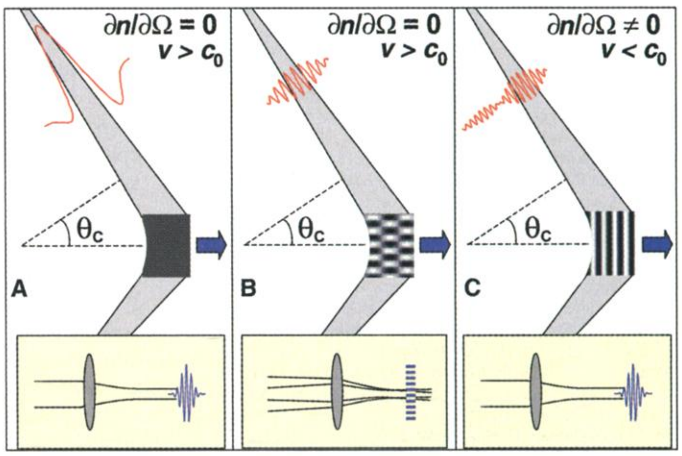

Fig. 4. Schematic diagrams of three methods used for generating Cherenkov fields. (**A**) and (**B**) represent Auston and co-workers' (*10*, *11*) and the traveling-grating method, which is the only one that relies on two pump beams. Our approach is illustrated in (**C**). The rectangular patterns are grayscale plots of the field in the vicinity of the pump pulse when the polarization source can be approximated by an infinitely extended plane. (A) and (B) require $v > c_0$ for phase matching.

ous approaches can now be described as follows. In Fig. 4, A and C, the angle between the polariton wave vector and the z axis is fixed, but not its magnitude. In the absence of dispersion, this leads to a shock-wave singularity because of the constructive interference of waves of arbitrary q. In Fig. 4B, both the angle and q are predetermined because the components of $\mathbf{q}$ orthogonal to $\mathbf{e}_z$ are set by the grating. These considerations apply to the imaging experiments of (*17*) and to early work on polariton propagation (*27*) where the direction of motion can be identified with that of the Cherenkov expression. Finally, consider single-pump excitation when the source lateral dimensions are sufficiently large that the wave vectors of the pump pulse and the polariton are nearly collinear. In this case, the phase-matching condition is $q \approx \Omega[n(\omega_L) + \omega_L \dot{n}(\omega_L)]/c \equiv \Omega/c_g(\omega_L)$. Because $q \approx \Omega/c_0$ at low frequencies, it is clear that phase matching can only be attained at subluminal speeds, in agreement with Eq. 6; see Fig. 2C. Under the same (quasi-planar) conditions, and not too far from the pump pulse, the field for the grating method results from the interference between two polaritons at, say, $q_x = \pm 2\pi/\ell$ and $q_y = 0$, where ℓ is the grating spacing (*12–17*). This and Eq. 7 give $q_z\ell = 2\pi(n^2v^2/c^2 - 1)^{-1/2}$, leading to $E \sim \sin(2\pi x/\ell)\sin[q_z(z - vt)]$. This field is represented in Fig. 4B by the rectangle with the checkerboard pattern (*28*).

References and Notes

1. V. P. Zrelov, *Cherenkov Radiation in High-Energy Physics* (Israel Program for Scientific Translations, Jerusalem, 1970).
2. T. Ypsilantis, J. Seguinot, *Nucl. Instrum. Methods A* **433**, 1 (1999), and references therein.
3. P. A. Cherenkov, *Dokl. Akad. Nauk SSSR* **2**, 451 (1934).
4. S. Vavilov, *Dokl. Akad. Nauk SSSR* **2**, 457 (1934).
5. I. Frank, *Vavilov-Cherenkov Radiation* (Nauka, Moscow, 1988).
6. ______, I. Tamm, *Dokl. Akad. Nauk SSSR* **14**, 109 (1937).
7. Expressions for the Cherenkov field in dispersive media were first derived by I. Tamm [*J. Phys.* **1**, 439 (1939)] and independently by E. Fermi [*Phys. Rev.* **57**, 485 (1940)], who used the Lorentz (single-pole) approximation to show that polarization effects lead to a reduction in the energy loss, a phenomenon known as the density effect. Ignoring dissipation, the condition for Cherenkov emission reads $v^2 > c^2/\varepsilon(\Omega)$. Because $\varepsilon(\Omega)$ can reach large values in the proximity of a resonance, a particle can in principle radiate at arbitrarily small velocities.
8. G. N. Afanasiev, V. G. Kartavenko, E. N. Magar, *Physica B* **269**, 95 (1999), and references therein. This work was motivated in part by recent CR experiments with CERN's high-energy beam of lead ions (*29, 30*).
9. To the best of our knowledge, the numerical study of Afanasiev *et al.* (*8*) was the first to uncover differences between superluminal and subluminal CR. In their work, these differences manifest themselves in the separate open ($v > c_0$) and closed ($v < c_0$) behavior of the surfaces at which the field exhibits maxima.
10. D. H. Auston, K. P. Cheung, J. A. Valdmanis, D. A. Kleinman, *Phys. Rev. Lett.* **53**, 1555 (1984), and references therein.
11. D. A. Kleinman, D. H. Auston, *IEEE J. Quantum Electron.* **QE-20**, 964 (1984).
12. P. Grenier, D. Houde, S. Jandl, L. A. Boatner, *Phys. Rev. B* **50**, 16295 (1994).
13. O. Albert, C. A. Gautier, J. C. Loulergue, J. Etchepare, *Solid State Commun.* **107**, 567 (1998).
14. H. J. Bakker, S. Hunsche, H. Kurz, *Rev. Mod. Phys.* **70**, 523 (1998), and references therein.
15. G. P. Wiederrecht *et al.*, *Phys. Rev. B* **51**, 916 (1995).
16. H. P. Perry, T. P. Doughtery, *Phys. Rev. B* **55**, 5778 (1997).
17. R. M. Koehl, S. Adachi, K. A. Nelson, *J. Chem. Phys.* **110**, 1317 (1999).
18. The calculations were performed with MATHEMATICA Version 4.0 (Wolfram Research, Inc., Champaign, IL, 1999).
19. The two regimes differ in that $\mathbf{E} \equiv 0$ outside the cone for the superluminal case, whereas, for $v < c_0$, the intensity does not vanish notwithstanding a substantial drop at the boundary. Hence, there is a shock-wave singularity at superluminal but not at subluminal speeds. The presence of a cone (as opposed to a plane) at $v < c_0$ contradicts the phase-velocity argument predicting $\theta_C = 0$ because c/nv can be arbitrarily close to unity.
20. Unlike the superluminal case, in which $\theta_C \leq \cos^{-1}(1/n_0)$, the Cherenkov angle for $v < c_0$ goes all the way to $\theta_C = \pi/2$ at $v = 0$. Also note that $d\varepsilon/d\Omega \to \infty$ at $\Omega = \Omega_C, \Omega_0$, which, according to Eq. 4, leads to $\alpha = 0$. Hence, at subluminal speeds, radiation at these frequencies is concentrated at $\rho = 0$.
21. See, e.g., Y. R. Shen, *The Principles of Nonlinear Optics* (Wiley, New York, 1984). Materials with infrared-active vibrations, such as ZnSe, show an additional contribution to the nonlinear polarization due to the combined phonon-photon character of the eigenmodes. The energy density becomes $-\Sigma\mathscr{E}_i\mathscr{E}_k(\chi^{(2)}_{ikm}E_m + R^{(m)}_{ik}Q_m)$, where $\mathscr{E}_K$ and E_m are electric field components of the pump pulse and that of the infrared radiation, Q_m is the amplitude of a phonon component, and $R^{(m)}$ is its associated Raman tensor.
22. H. Li, *J. Phys. Chem. Ref. Data* **13**, 102 (1984).
23. Values of the infrared constants of ZnSe from the literature exhibit considerable scattering. Those in Fig. 2 were interpolated from measurements at 80 K (*22*) and at 2 K [A. Göbel, T. Ruf, J. M. Zhang, R. Lauck, M. Cardona, *Phys. Rev. B* **59**, 2749 (1999); T. Hattori, Y. Homma, A. Mitsuishi, M. Tacke, *Opt. Commun.* **7**, 229 (1973)]. Data for n in the visible range are available at temperatures above 90 K (*22*). Values at 10 K were obtained from an expression giving $n(\Omega)$ in terms of the band gap, the carrier effective masses, and the value of n at the gap [B. Jensen, A. Torabi, *Infrared Phys.* **23**, 359 (1983)]. The latter was used as an adjustable parameter to fit the time-domain data.
24. T. E. Stevens, thesis, University of Michigan, Ann Arbor (2000).
25. M. Born, K. Huang, *Dynamical Theory of Crystal Lattices* (Clarendon, Oxford, 1996), p. 100.
26. We used heterodyne detection methods. The pump beam was modulated with a mechanical chopper at 3.51 kHz. The transmitted probe light was analyzed with a polarizing beam cube and spectrally resolved (*24*). The probe beam and a reference beam, also dispersed by the spectrometer, were focused onto separate photodiodes, and their voltage difference was measured with a dual channel EG&G 5320 digital lock-in amplifier to get ΔT.
27. G. M. Gale, F. Vallée, C. Flytzanis, *Phys. Rev. Lett.* **57**, 1867 (1986).
28. In (*14*), pump-probe data for polaritons generated with a traveling grating were interpreted in terms of avoided mode crossings and anharmonicity. Given that Cherenkov field profiles can be fairly complicated, there may be a need to compare the experiments with calculations of the field due to a finite traveling grating before such interpretations can be accepted.
29. V. P. Zrelov, J. Ruzicka, A. A. Tyapkin, *JINR Rapid Commun.* **1[87]-98**, 23 (1998).
30. V. P. Zrelor, J. Ruzicka, A. A. Tyapkin, *CERN Courier* **38** (no. 9), 7 (1998)].

31. We are grateful to C. Aku-Leh for assistance with the calculations and to D. G. Steel for critical reading of the manuscript. T.E.S. would like to thank the Max-Planck-Institut für Festkörpertorschung for warm hospitality. Work supported by the NSF under grant DMR 9876862 and by the Air Force Office of Scientific Research under contract F49620-00-1-0328 through the Multidisciplinary University Research Initiative program.

29 September 2000; accepted 30 November 2000

Directed Assembly of One-Dimensional Nanostructures into Functional Networks

Yu Huang,[1*] Xiangfeng Duan,[1*] Qingqiao Wei,[1] Charles M. Lieber[1,2†]

One-dimensional nanostructures, such as nanowires and nanotubes, represent the smallest dimension for efficient transport of electrons and excitons and thus are ideal building blocks for hierarchical assembly of functional nanoscale electronic and photonic structures. We report an approach for the hierarchical assembly of one-dimensional nanostructures into well-defined functional networks. We show that nanowires can be assembled into parallel arrays with control of the average separation and, by combining fluidic alignment with surface-patterning techniques, that it is also possible to control periodicity. In addition, complex crossed nanowire arrays can be prepared with layer-by-layer assembly with different flow directions for sequential steps. Transport studies show that the crossed nanowire arrays form electrically conducting networks, with individually addressable device function at each cross point.

Nanoscale materials, for example, nanoclusters and nanowires (NWs), represent attractive building blocks for hierarchical assembly of functional nanoscale devices that could overcome fundamental and economic limitations of conventional lithography-based fabrication (*1–4*). Research focused on zero-dimensional nanoclusters has led to substantial advances, including the assembly of arrays with order extending from nanometer to micrometer length scales (*4–9*). In contrast, the assembly of one-dimensional (1D) nano-